frontiers in Materials

ORIGINAL RESEARCH
published: 18 January 2022
doi: 10.3389/fmats.2021.710155

Microwave-Assisted Green Synthesis of Pure and Mn-Doped ZnO Nanocomposites: *In Vitro* Antibacterial Assay and Photodegradation of Methylene Blue

Sher Bahadar Khan[1]*, *Muhammad Iqbal Khan*[2] and *Jamila Nisar*[2]

[1]Department of Chemistry, King Abdulaziz University, Jeddah, Saudi Arabia, [2]Department of Chemistry, Kohat University of Science and Technology, Kohat, Pakistan

This paper describes the eco-friendly microwave-assisted green synthesis of pure and manganese-doped zinc oxide nanocomposites using ethanolic solution of castor oil as a reductant and capping agent. Solutions of Zn^{2+} and Mn^{2+} ions were mixed in fixed ratios to obtain 0%, 1%, 2.5%, 5%, and 7% pure and Mn-doped ZnO nanomaterials. The obtained nanomaterials were characterized by powder XRD, FT-IR spectroscopy, scanning electron microscopy, and EDX analyses. Powder XRD furnished characteristic fragmentation patterns for the confirmation of the synthesized materials and was also used to estimate the size of the synthesized nanoparticles by Scherrer's equation. Diffraction patterns were characteristic of wurtzite structure and of the size in the range of 6.5, 5.6, 5.2, 5.1, and 4.3 nm for pure and Mn-doped ZnO nanocomposites. UV-visible spectra displayed maximum absorbance at 340 nm, and manganese doping caused a red shift. FT-IR spectra confirmed that the formation of zinc oxide nanoparticles as Zn–O appeared at below 700 cm^{-1} as well as the presence of organic moieties of the castor oil acting as stabilizing agents. Scanning electron micrographs (SEM) revealed all the synthesized materials were spherical in shape with some aggregation and polydispersity, and in the Energy-dispersive X-ray spectroscopy (EDX), specific peaks with characteristic patterns were seen for Zn, O, and Mn. A TEM micrograph displayed the hexagonal wurtzite structure of nanoparticles with average size less than 50 nm. Photocatalytic degradation of methylene blue was checked in the presence of sunlight and in darkness. Interestingly, samples placed under the solar radiation exhibited significant results only with the catalyst; all the samples used without the catalyst showed negligible degradation effects, and even the samples placed in the dark containing catalysts also displayed a negative effect. A mechanism for this significant activity is also proposed. *In vitro* the antibacterial potential was studied against two pathogenic strains, i.e., *Streptococcus aureus* and *Escherichia coli*; interestingly activity kept on increasing with the increasing manganese content. Overall, all the samples presented comparable activity to ciprofloxacin.

Keywords: Mn-doped ZnO, microwave, castor oil, methylene blue, solution kinetics

OPEN ACCESS

Edited by:
Ahmed A. Abdala,
Texas A&M University at Qatar, Qatar

Reviewed by:
Ratiram Gomaji Chaudhary,
Seth Kesarimal Porwal College, India
Saviour A. Umoren,
King Fahd University of Petroleum and Minerals, Saudi Arabia

****Correspondence:***
Sher Bahadar Khan
sbkhan@kau.edu.sa

Specialty section:
This article was submitted to Polymeric and Composite Materials, a section of the journal Frontiers in Materials

Received: *15 May 2021*
Accepted: *22 October 2021*
Published: *18 January 2022*

Citation:
Khan SB, Khan MI and Nisar J (2022) Microwave-Assisted Green Synthesis of Pure and Mn-Doped ZnO Nanocomposites: In Vitro *Antibacterial Assay and Photodegradation of Methylene Blue. Front. Mater. 8:710155. doi: 10.3389/fmats.2021.710155*

INTRODUCTION

Nanoscale materials have grabbed the attention of researchers due to their novel properties, which are not observed in their bulk-sized analogues (Jang et al., 2011; Khan et al., 2016a; Khan et al., 2016b; Taloni et al., 2018; Pryazhnikov and Kubrakova, 2021). Therefore, they have been applied in various fields (Kim et al., 2016; Gul et al., 2017; Kamal et al., 2017; Ismail et al., 2018; Han et al., 2019). Metal oxide nanoparticles are widely used owing to their unique characteristics, such as ductility, optical, magnetic, sensitivity, catalysis etc. (Chouke et al., 2019; Sonkusare et al., 2018; Khan et al., 2015a). Due to these unique properties, metal oxide nanoparticles have attracted researchers working in the field of materials, agriculture, chemical sciences, environment, and information technology (Khan et al., 2015b; Ahmad et al., 2017; Bashir et al., 2019; Frank et al., 2020).

Nanoscale zinc oxide exhibits interesting optical, catalytic, optoelectronic, and photocatalytic properties like rest of the metal oxides (Bandeira et al., 2020). Zinc oxide nanoparticles are also common ingredients of cosmetics and sunscreens due to their efficient absorbance of ultraviolet light. Interestingly, they are highly transparent to visible light; on the contrary, micro- and sub-micrometer counterparts lack this combination of properties (Ahmad et al., 2019; Vinci and Rapa, 2019; Bashir et al., 2020). Synthesis and use of zinc oxide nanoparticles at such an elevated level also increase their exposure to humans and the environment (Singh et al., 2018; Alosman et al., 2021). Recently, investigators have analyzed the toxicity of zinc oxide nanoparticles toward mice; the mechanism of cytotoxicity includes the interaction of cells resulting in the production of reactive oxygen species (Pandurangan and Kim, 2015; Nazir et al., 2020).

Manganese doping of zinc oxide, which is a *p*-type semiconductor, may lead to the development of room temperature ferromagnetic material with potential use in spintronics—the next-generation nano-electronic devices. Efforts are also underway to develop zinc oxide and its doped products for their use in photocatalysis and biological sensing phenomena (Singh et al., 2019). Manganese is the first transition metal dopant for zinc oxide nanoparticles due to its larger magnetic moment. Additionally, the biocompatibility and structural diversity of zinc oxide nanoparticles makes it an excellent core material (Czyżowska and Barbasz, 2020). Another advantage of utilizing manganese as a dopant metal is its effectiveness in enhancing thermal, optical, and photocatalytic character without affecting the basic hexagonal structure of zinc oxide. It is worth mentioning that, despite the importance of the magnetic properties of manganese doping, few reports dealing with the photocatalytic and antibacterial studies of manganese-doped zinc oxide nanoparticles are available (Lee et al., 2016; Thakur et al., 2020; Biswas et al., 2021).

Based on these facts, we report a microwave-assisted green synthesis of pure and manganese-doped (1%, 2.5%, 5%, and 7%) zinc oxide nanocomposites using for the first time castor oil as a surface stabilizing agent. The synthesized materials were thoroughly characterized and applied for photocatalytic degradation of methylene blue (MB), and *in vitro* antibacterial activity was performed on *Streptococcus aureus* and *Escherichia coli*.

MATERIALS AND METHODS

Materials

$Zn(CH_3COO)_2.2H_2O$, $MnCl_2.2H_2O$, NaOH, C_2H_5OH, and MB were obtained from BDH, England, and nutrient agar was procured from Oxoid Ltd. (England). Castor oil was purchased from a local grocery store.

Instrumentation

Morphology of the synthesized samples was studied with a field emission scanning electron microscope of JEOL (JSM-7600F, Japan); elemental analyses were investigated by the JSM-7600F system, Japan; FT IR spectra were acquired on a PerkinElmer spectrophotometer (Spectrum 100) in the range 400–4000 cm^{-1}; and diffraction patterns were recorded on a powder X-ray analytical diffractometer PAN (JDX-3532 JEOL, Japan).

Microwave-Assisted Green Synthesis of ZnO Nanoparticles

$Zn(CH_3COO)_2.2H_2O$ was used as a Zn^{2+} source, and castor oil was employed as a green reagent for capping and reducing purposes. Briefly, 25 mM (5.4877 g) aqueous solutions of zinc acetate and 1 mM NaOH were prepared in 50 ml separately in deionized water. Then, 15 ml ethanol and 15 ml castor oil were mixed to obtain a homogeneous solution and added to the NaOH solution. This mixture was then added to the $Zn(CH_3COO)_2.2H_2O$ solution. The prepared mixture was then placed inside a commercial household microwave oven (2.5 GHz) for 150 s, resulting in the appearance of a milky white product; the white solid was centrifuged and then washed thrice with deionized water, ethanol, and finally acetone and oven dried at 100°C. Finally, the dried powder was calcined at 200°C for 4 h in a furnace.

Microwave-Assisted Green Synthesis of Mn-Doped ZnO Nanocomposites

Mn-doped ZnO nanocomposites were synthesized in a similar way as discussed above for the synthesis of ZnO nanoparticles. Briefly, 15 ml castor oil and 15 ml ethanol mixture were consumed as a green reductant and capping agent in these reactions. A few drops of 1 mM NaOH were added to maintain the basic pH of the reaction medium to aid the synthesis process; to prepare Mn-doped ZnO nanocomposites, aqueous solutions of $Zn(CH_3COO)_2.2H_2O$ and $MnCl_2$ were mixed in fixed ratios (1%, 2.5%, 5%, and 7%); samples were dried at 100°C, and the dried powder was calcined at 200°C for 4 h in a furnace.

Photocatalytic Degradation of MB

The synthesized nanomaterials were employed to study the photocatalytic degradation of MB irradiated by UV light on a UV/visible spectrophotometer (Shimadzu 1800, Japan) with slight modifications as reported in the literature (Dutta et al., 2015). Briefly, 20 mg of synthesized nanomaterials were added to 0.1 mM (50 ml) solution of MB in a beaker. After addition of nanomaterials, the mixture was kept in a dark place for 10 min, and stirring was

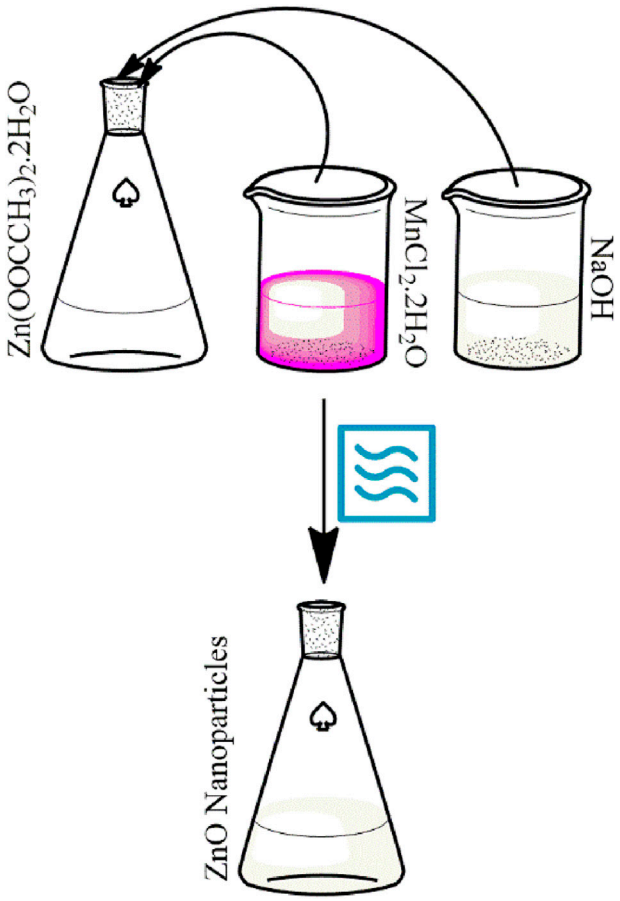

Scheme 1 | Schematic representation for green synthesis of pure and Mn-doped ZnO.

continued to obtain absorption-desorption equilibrium. The solution was divided into two equal portions. One portion was placed in darkness at 28°C, and the second portion was placed in sunlight at 45°C. UV-visible spectra of centrifuged solutions were recorded at regular intervals of time, i.e., 10, 30, and 60 min.

In vitro Antibacterial Screenings

The prepared nanoparticles were screened for *in vitro* antibacterial activity, For the antibacterial activity of zinc oxide nanoparticles, the agar-well diffusion protocol was applied using ciprofloxacin as a reference drug for two bacterial strains, viz. *Staphylococcus aureus* (gram positive) and *Escherichia coli* (gram negative) were used. Comparative analysis of zones of inhibition of the bacterial strains was carried out with the reference drug (Rahman et al., 2001; shah et al., 2013; Khan et al., 2020).

RESULTS AND DISCUSSION

Synthesis of Pure and Mn-Doped ZnO Nanocomposites

Green synthesis of pure and Mn-doped ZnO nanocomposites was carried out successfully with the use of castor oil as a capping agent and microwaves for the completion of the reactions as shown in **Scheme 1**.

Interestingly, the color of ZnO became deeper with the increasing percentage of Mn-dopant as evident in the macrographs in **Figure 1**. ZnO presented a white color, and the addition of 1% Mn as a dopant turned it darker; further systematic addition of Mn dopant deepened the coloration.

Characterization of the Synthesized Materials

The formation of pure and Mn-doped ZnO nanocomposites was verified by a UV-visible spectroscopic method (**Figure 2**). UV-Vis spectra were recorded in deionized water showing maximum absorption at 338 nm for pure ZnO; nanoparticles displayed maximum absorption at 338 nm, which confirmed the formation of pure ZnO nanoparticles (Fang et al., 2004). All the Mn-doped nanoparticles showed maximum absorption lower than 400 nm, and according to the literature, nanoscale ZnO absorbs UV-Vis light in this wavelength region (Tănase et al., 2021). In the UV-Vis spectra of Mn-doped ZnO nanocomposites (1%, 2.5%, 5%, and 7%), a red shift in the absorption edge was observed, and it may be owing to the decrease in the crystallite size of nanoparticles, morphology, surface

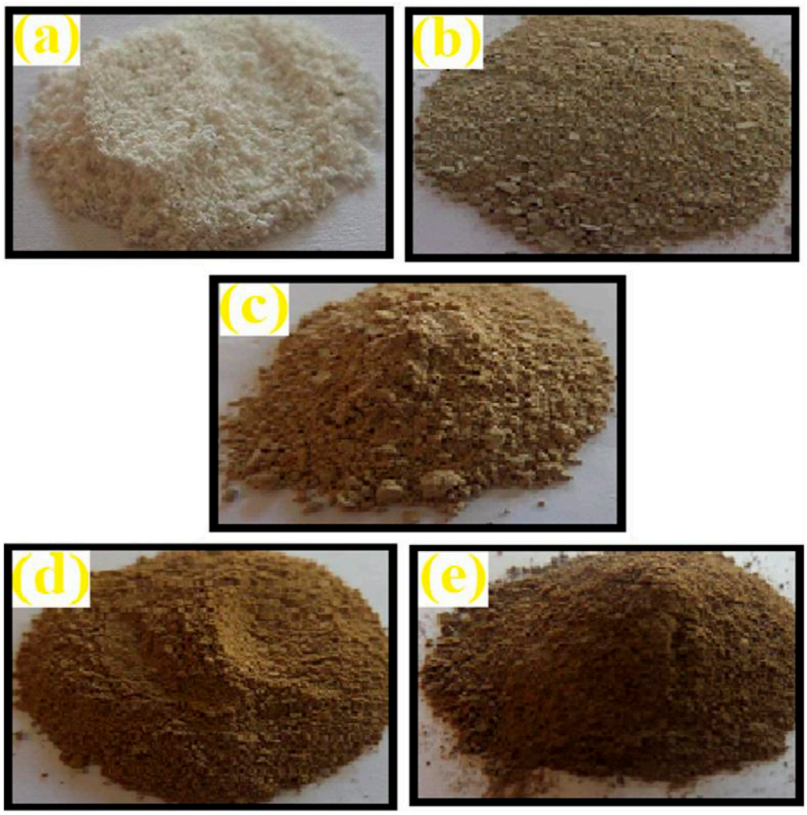

FIGURE 1 | Macrographs of pure ZnO **(A)** and Mn-doped 1% **(B),** 2.5% **(C)**, 5% **(D)**, 7% **(E)** ZnO nanomaterials.

effects caused by increasing dopant concentration, and Mn clustering. The band gap energy (E_{bg}) was calculated with the help of formula $E_{bg} = hc/\lambda$ (h: Planck's constant = 4.135667 × 10^{-15} eV s, and c: velocity of light = 2.997924 × 10^{8} m/s; λ: absorbance wavelength nm); obtained values of the band gap were 3.66 eV (ZnO), 3.63 eV (1% Mn-doped ZnO), 3.62 eV (2.5% Mn-doped ZnO), 3.61 eV (5% Mn-doped ZnO), and 3.6 eV (7% Mn-doped ZnO), respectively. This may be attributed to the very insignificant changes between the magnetic and optical properties of the Mn-doped ZnO nanocomposites. Moreover, an improvement in the ferromagnetic order with increased Mn doping was observed with the increasing dopant concentration, and this is due to ferromagnetic coupling of the Mn-dopant. The same accounted for the observation of a "red shift" as well as bowing due to a direct band gap and increased saturation of magnetization with the increasing Mn-dopant level (Lang et al., 2010; Karmakar et al., 2013).

FT-IR spectroscopy is an essential tool to investigate various functional groups present in the castor oil molecules acting as a capping agent. In the FT-IR spectra of pure and Mn-doped (1%, 2.5%, 5%, and 7%) ZnO nanoparticles, typical peaks were observed at 3442 cm^{-1}, 1556 cm^{-1}, 1338 cm^{-1}, 1080 cm^{-1}, and 825–665 cm^{-1}. A broad band at 3442–3332 cm^{-1} showed stretching vibration due to the O–H group, confirming the presence of physiosorbed moisture at the surface of the metal nanoparticles. A band at 1338 cm^{-1} was observed, indicating the presence of C=O asymmetric stretching vibration, and the two other bands at 1556 cm^{-1} and 1080 cm^{-1} may be due to stretching vibration of the C–O group, confirming the presence of the organic capping agent at the surface of the ZnO nanoparticles (Biswas et al., 2021). The band obtained at 825 cm^{-1} confirmed the formation of four-coordinated zinc complexes, and bands below 1000 cm^{-1} were assigned to Mn–O stretching vibration. A broad band at 665 cm^{-1} confirmed Zn–O stretching vibrations (Almehizia et al., 2021). To conclude the discussion, the presence of organic moieties from castor oil included the presence of aromatic amines and O–H due to the presence of moisture on the surface of synthesized nanoparticles.

The structure of microwave-assisted green synthesized pure and Mn-doped ZnO nanocomposites was confirmed by Powder XRD analysis as revealed in **Figure 3**. Diffraction patterns exhibited seven intense peaks in the range of 20–70 of the complete spectrum of 2θ value. XRD patterns show these diffraction peaks at 31.9, 34.5, 36.4, 47.6, 56.8, 62.9, 68.0 position of the 2θ value, and these correspond to their characteristic Bragg peaks of (100), (002), (101), (102), (110), (103) and (112) (Pathak et al., 2016; Zhan et al., 2021). These characteristic peaks correspond to the hexagonal or wurtzite structure of ZnO NPs and Mn-doped ZnO nanoparticles (Pathak and Swart, 2019) as shown in the JCPDS card no.80-0075. The average crystallite size of the synthesized nanoparticles was calculated by using the Scherrer equation.

$$D = k\lambda/\beta \cos\theta,$$

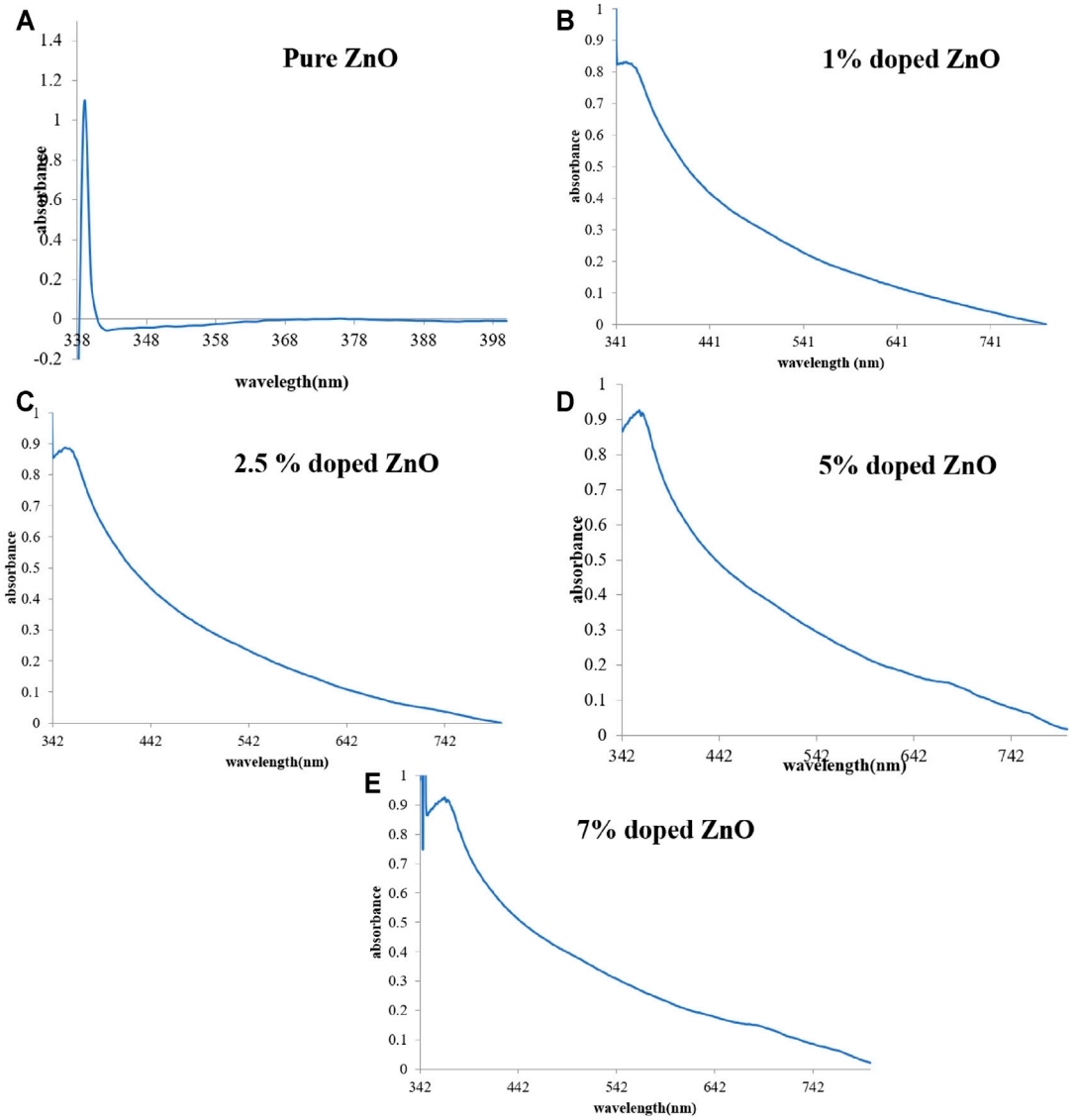

FIGURE 2 | UV-Vis spectra of pure ZnO **(A)** and Mn-doped 1% **(B)**, 2.5% **(C)**, 5% **(D)**, 7% **(E)** ZnO nanomaterials.

where k is constant (0.94), λ is the wavelength of X-rays used (1.5418 Å), and β is the FWHM of the most intense peak.

The average crystallite size was calculated by full width at half maximum (FWHM) for the most intense peak corresponding to (101). Bragg's peak of pure ZnO nanoparticles was 8.8 nm, and for Mn-doped ZnO nanocomposites, values of 6.5, 5.7, 5.6, and 4.3 nm were obtained for 1%, 2.5%, 5%, and 7%, respectively.

Surface morphology and shapes of the synthesized pure and Mn-doped ZnO nanocomposites were determined by scanning electron microscopy (SEM). In materials research, the surface morphology and shape of metallic nanoparticles is routinely investigated by SEM. SEM micrographs of the synthesized ZnO nanoparticles and Mn-doped ZnO nanocomposites showed that the pure nanoparticles of ZnO were spherical and oval. Examination of the SEM micrographs of the synthesized materials displayed these as granular and somewhat oval in shape with a coarse surface, which indicates the presence of the capping agents on the surface. SEM micrographs of Mn-doped ZnO nanocomposites showed that the synthesized nanoparticles were poly-dispersed aggregates, roughly spherical, lacking mono-dispersity as shown clearly in **Figure 4** (Abdollahi et al., 2011; Ahmad et al., 2020a; Ahmad et al., 2020b) although the TEM micrograph displayed a hexagonal wurtzite structure of pure ZnO nanoparticles with average size around 50 nm. The influence of manganese content, i.e., 1%, 2.5%, 5%, and 7%, on the morphological changes was also observed, and an increase in manganese content increased the grain size. This may be attributed to nucleation of higher concentration manganese with oxygen and formation of bigger particles. Consequently, particles with lower manganese concentrations displayed lower agglomeration than the higher manganese concentration as dopant (Yang et al., 2010; Al-Kordy et al., 2021).

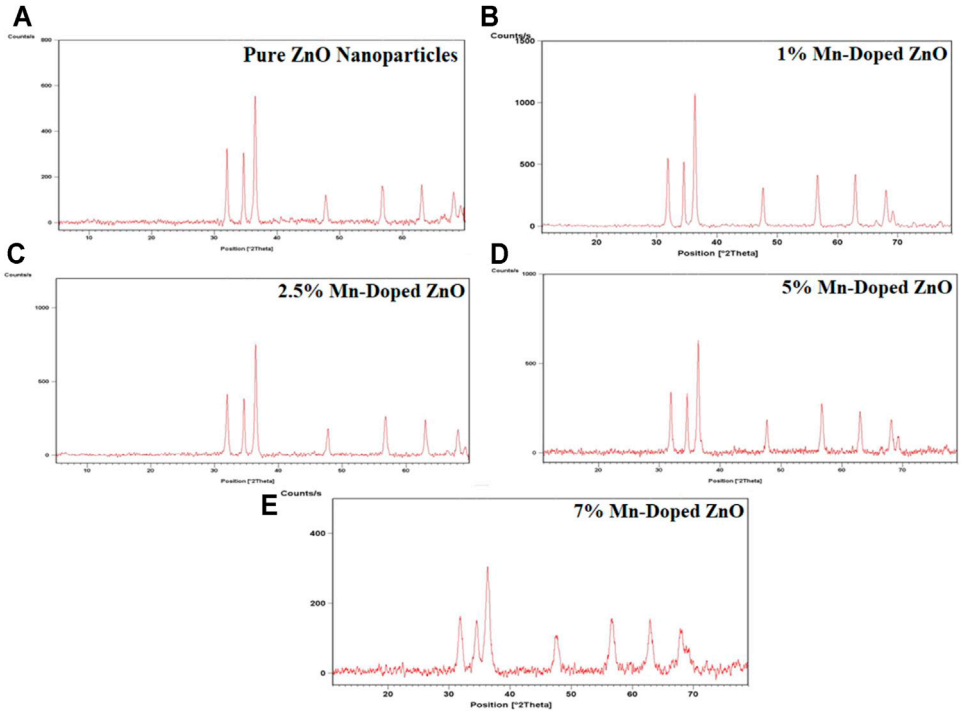

FIGURE 3 | Powder X-ray diffraction patterns of the synthesized pure and Mn-doped ZnO nanocomposites.

EDX, which was carried out for the elemental analysis of the synthesized samples, confirmed the presence and purity of the prepared nanocomposites. EDX analysis presented in **Figure 5** clearly indicates the composition of the synthesized nanoparticles was almost like the stoichiometric ratios. The EDX spectrum (**Figure 5A**) for pure ZnO nanoparticles showed a strong peak for Zn at 1, and 9 keV confirmed the presence of Zn. It also showed a peak of O, which confirmed the sample was pure and contained only O and Zn. On the other hand, the EDX spectra (**Figures 5B–E**) for Mn-doped ZnO nanocomposites (1%, 2.5%, 5%, 7%) displayed an additional peak for Mn at 6 keV along with the peaks for O and Zn, confirming that the doping successfully took place in the given stoichiometry. It is evident from **Figures 5B–E** that the Mn percentage in stoichiometry was regularly increasing with doping enhancement (Khan et al., 2017).

Photocatalytic Degradation of MB

MB is a dye used in the coloring of paper, artificial hair, fabrics, etc., and it causes toxic effects on humans (Nazir et al., 2020), which prompted us to study the photocatalytic degradation of MB. In this degradation process, pure ZnO was used as photocatalyst by employing the typical absorbance of MB at 664 nm as a monitoring reference for monitoring this property of all the synthesized samples.

Photocatalytic degradation activity of ZnO nanoparticles was evaluated with and without light at different time intervals (10, 30, and 60 min) as shown in **Figures 6A,B**. It is very clear from the figures that the photocatalytic degradation of MB had taken place efficiently by the synthesized samples.

In the reaction that took place under the light, the spectrum for MB without any catalyst was at 663 nm, having absorbance intensity 3.3, which was the same as in the reaction without light, showing that the concentration of MB was identical. Furthermore, no degradation took place until the catalyst was added to the MB solution. The degradation activity in the absence of light was not very satisfactory although the photodegradation in light presented better results for MB up to 70% as shown in **Figure 6**. Generally, it was obvious that, by increasing the contact and illumination times of MB, the absorption was reduced, confirming the degradation of MB. The results demonstrate that ZnO nanoparticles showed a catalytic performance at different time intervals on photodegradation of MB. The total degradation achieved by ZnO in the reaction in the presence of light was 70% in 60 min, proving that ZnO adequately influences the process and is a proficient catalyst in photodegradation of MB as compared with reported materials (Anju Chanu et al., 2019).

The kinetics of the photocatalyst toward MB degradation was investigated and followed a pseudo-first order rate as given in the following equation:

$$\ln C_t/C_o = \ln At/Ao - Kt,$$

where C_t is the concentration of MB, which equal to the absorbance value at the designated time, and C_o is absorbance at time (t) = 0. K is the rate constant of the reaction and was measured by the linear fitting of $\ln C_t/C_o$ versus t. The plot of $\ln C_t/C_o$ is functional of time of MB degradation by ZnO nanoparticles (**Figure 6D**). The rate constant for MB degradation by the photocatalyst was calculated as 0.0192 min^{-1}.

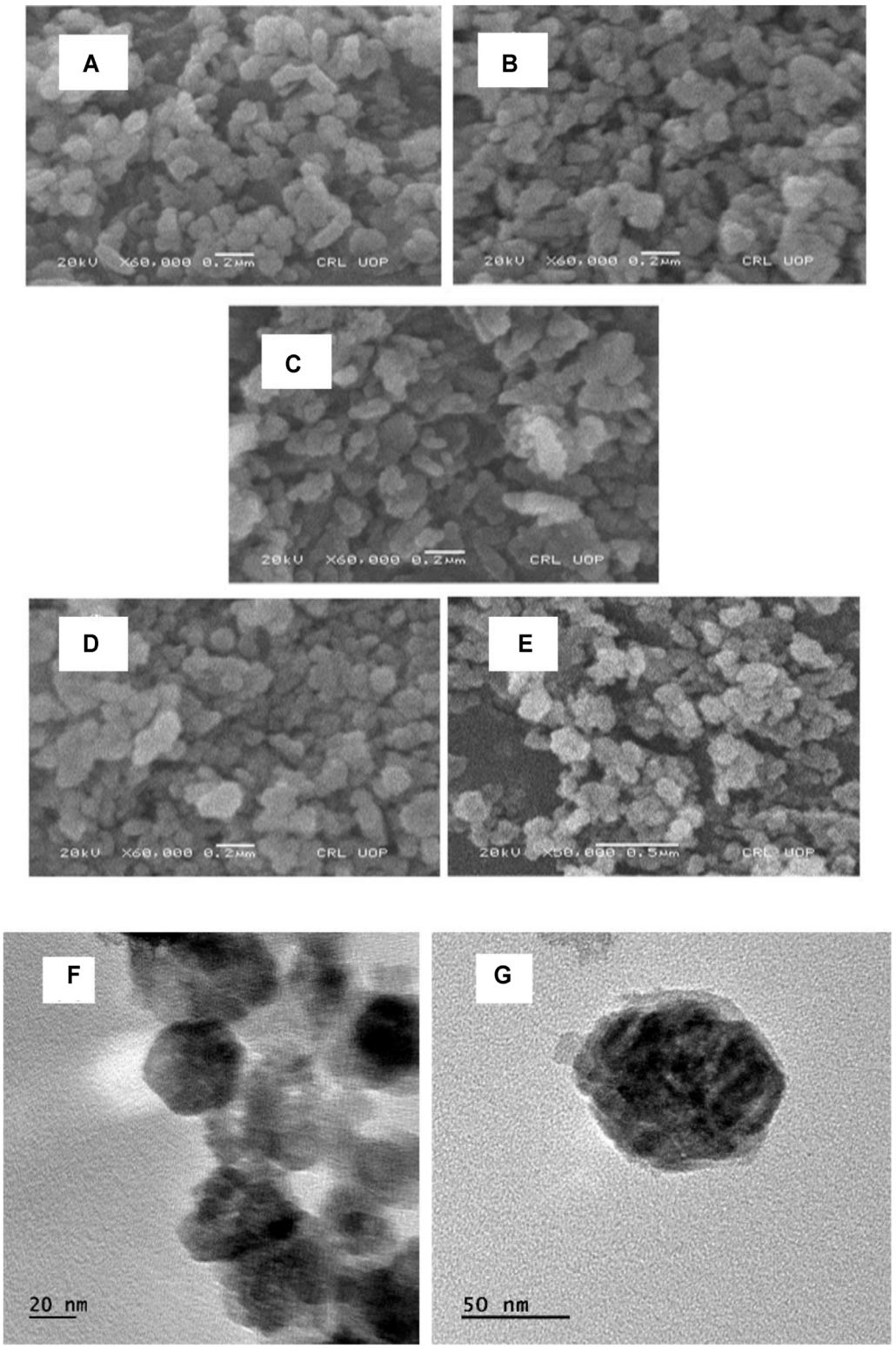

FIGURE 4 | SEM micrographs of pure ZnO **(A)** and Mn-doped ZnO [**(B)**:1%, **(C)**:2.5%, **(D)**: 5% and **(E)**:7%) nanocomposites; TEM micrographs of ZnO NPs **(F, G)]**.

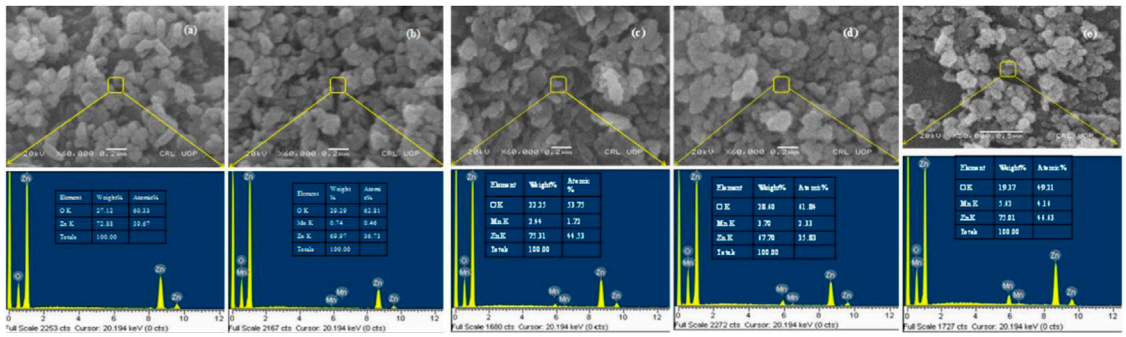

FIGURE 5 | EDX analysis of **(A)** pure ZnO and **(B–E)** Mn-doped [**(B)**:1%, **(C)**:2.5%, **(D)**: 5% and **(E)**: 7%)] ZnO nanocomposites.

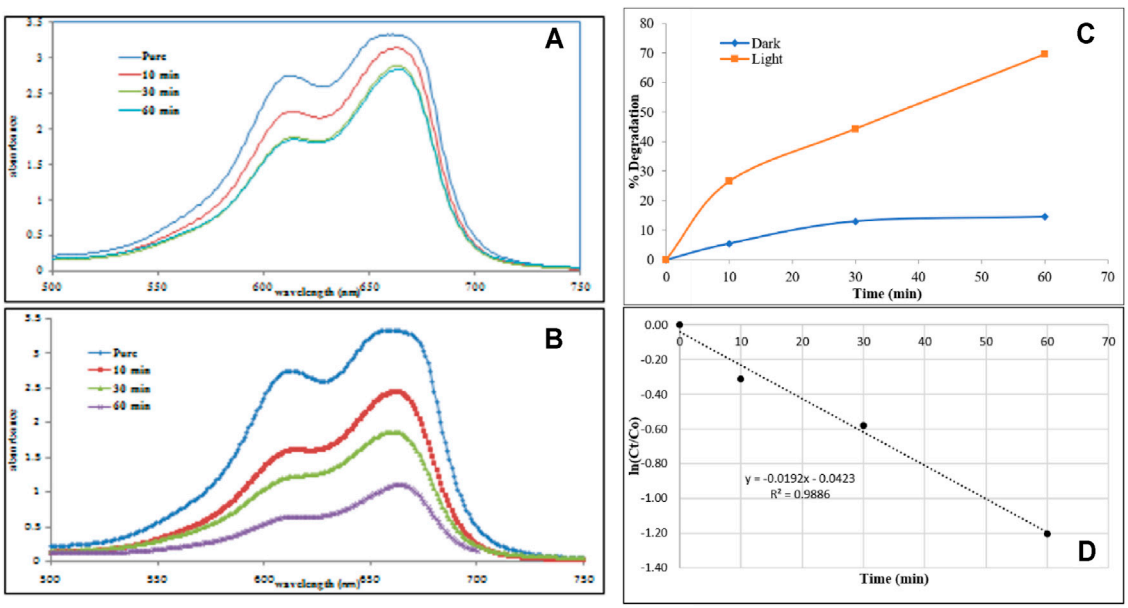

FIGURE 6 | Degradation activity of ZnO nanoparticles on MB **(A)** in absence of light **(B)** in presence of light **(C)** comparative percent reduction, and **(D)** kinetics of MB degradation.

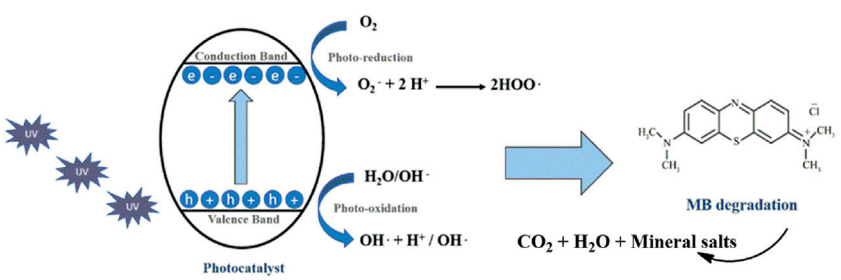

FIGURE 7 | Schematic representation of mechanism for degradation of MB using photocatalyst.

The mechanism of photocatalytic degradation of MB dye is schematically shown in **Figure 7**. Initially, ZnO absorbs light energy greater than or equal to the band gap energy, and then an electron from the valence band gets excited to the conduction band and leaves a positive charge hole in the valence band. The electron in the excited state reacts with atmospheric oxygen and

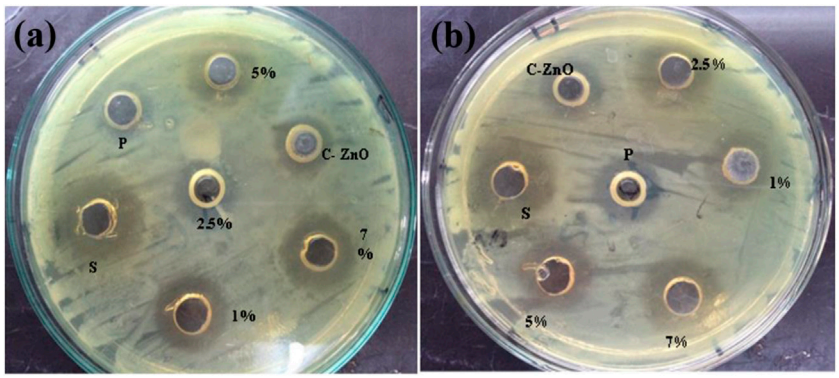

FIGURE 8 | Comparison of antibacterial activity of standard antibiotic drug (*ciprofloxacin*), bulk ZnO, and pure ZnO nanoparticles as well as 1%, 2.5%, 5%, and 7% Mn-doped against **(A)** *S. aureus* and **(B)** *E. coli*.

TABLE 1 | *In vitro* dose-dependent comparative (zone of inhibition in millimeters) antibacterial assay of pure and Mn-doped ZnO NPs with MIC in parenthesis (zone of inhibition, mM).

Materials	Concentration	Zone of inhibition (mm, n: 3, MIC in mM)	
		E. coli	*S. aureus*
Undoped ZnO NPs	(1 mg/50 µL)	8.6 ± 0.07 (0.92)	10.1 ± 0.0.12 (0.96)
	(5 mg/50 µL)	9 ± 0.1 (0.97)	10.4 ± 0.21 (1.02)
1% Mn-doped ZnO NPs	(1 mg/50 µL)	11 ± 0.31 (0.52)	13.3 ± 0.08 (0.66)
	(5 mg/50 µL)	12.8 ± 0.23 (0.41)	15.2 ± 0.21 (0.81)
2.5% Mn-doped ZnO NPs	(1 mg/50 µL)	13.3 ± 0.05 (0.44)	16.3 ± 0.32 (0.8)
	(5 mg/50 µL)	13.9 ± 0.08 (0.4)	17 ± 0.11 (0.76)
5% Mn-doped ZnO NPs	(1 mg/50 µL)	14.2 ± 0.03 (0.41)	16.8 ± 0.28 (0.75)
	(5 mg/50 µL)	14.4 ± 0.07 (0.42)	17.3 ± 0.28 (0.77)
7% Mn-doped ZnO NPs	(1 mg/50 µL)	15.1 ± 0.28 (0.5)	18.1 ± 0.09 (0.79)
	(5 mg/50 µL)	15.4 ± 0.28 (0.5)	18.3 ± 0.11 (0.8)
Ciprofloxacin	(5 µg/50 µL)	41.2 ± 0.22	31 ± 0.17

produces a superoxide radical as a reactive species. These reactive species further produce free radicals as given in **Figure 7**, which completely degrades MB dye. The mechanism proposed for MB degradation is ably supported by the calculated values of band gap energy; also, the morphological analysis proved to be supportive of this surface area, thereby making the reported nanoparticles a promising candidate for the solar light–induced photocatalytic degradation of MB.

In vitro Antibacterial Activity of the Synthesized Materials

The antibacterial activity of ZnO NPs was tested against two pathogenic strains, which were gram-positive *S. aureus* and gram-negative *E. coli*. Ciprofloxacin was used as a standard antibiotic drug using the disc diffusion method. The increase in fold area was deliberated using the following equation:

$$\text{Increase in fold area} = \frac{B^2 - A^2}{A^2},$$

where A is the zone of inhibition for the standard antibiotic, and B is the zone of inhibition of bulk ZnO (**Figure 8**), synthesized pure ZnO nanoparticles, and Mn-doped ZnO nanoparticles (Sharma et al., 2016; Mesaros et al., 2019). The zone of inhibition of all synthesized samples of nanoparticles, our standard antibiotic drug (ciprofloxacin), and ZnO (bulk) are given in **Table 1**.

It is clear from the results that the prepared samples have antibacterial activity against the two test strains of bacteria. ZnO nanoparticles were greater than that of the bulk-scale ZnO, and there was also an increase in antibacterial activity as dopant percentage increases as shown in **Figure 8**. The antibacterial activity of the synthesized nanoparticles furnished an interesting trend, i.e., with the increasing dopant concentration, the activity also showed an upward trend with the highest dopant concentration sample exhibiting the highest activity comparable to the reference drug ciprofloxacin. This is in accordance with the literature supporting increasing dopant concentration resulting in enhanced activity (Duman et al., 2020). The antibacterial activity of pure and Mn-doped ZnO nanoparticles was compared as a function of increasing dopant concentrations by evaluating the zone of inhibition. Inhibition zone sizes (millimeters) were noted against either *E. coli* and *S. aureus* and shown in **Table 1**. By increasing dopant concentration, a positive charge at the surface of the ZnO increases, which helps these materials to effectively interact with

negative charge points of the cell membrane. That halts the vital cell wall functions, such as permeability and respiration, thereby compromising its integrity, and ultimately leads to the breakdown of the cell (Braydich-Stolle et al., 2005).

CONCLUSIONS

The green synthesis of pure and manganese-doped zinc oxide nanoparticles is carried out successful by using microwaves and castor oil as a reducing as well as stabilizing agent. UV-visible spectra were employed to study the course of the reaction; the presence of different functional groups from castor oil was confirmed by FTIR spectra. Band gap energy was calculated from UV-visible spectra, and it is concluded from the UV-visible spectra, and the trend was corroborated by SEM morphological analysis. Mn-doped ZnO proved to be an excellent photocatalyst under solar light for the degradation of MB dye. As expected, Mn doping proved to be decisive in enhancing photocatalytic potential although a similar promising trend was observed during the *in vitro* antibacterial activity screening results. *In vitro* antibacterial screenings provided a correlation between size and activity, i.e., the smaller the size, the greater the activity, and the dopant concentration played a role in size reduction, which ultimately led to an enhancement in activity.

DATA AVAILABILITY STATEMENT

The original contributions presented in the study are included in the article/Supplementary Material, further inquiries can be directed to the corresponding author.

AUTHOR CONTRIBUTIONS

SK have prepared the materials. MK and JN performed photocatalytic degradation and antibacterial activity. All authors wrote, read, and approved the final manuscript.

FUNDING

This project was funded by the Deanship of Scientific Research (DSR) at King Abdulaziz University, Jeddah, under grant no. G: 682-130-1441. The authors, therefore, acknowledge with thanks DSR for technical and financial support.

REFERENCES

Abdollahi, Y., Abdullah, A. H., Zainal, Z., and Yusof, N. A. (2011). Synthesis and Characterization of Manganese Doped ZnO Nanoparticles. *Int. J. Basic Appl. Sci.* 11, 62–69. doi:10.1021/jp049960o

Ahmad, I., Khan, S. B., Kamal, T., and Asiri, A. M. (2017). Visible Light Activated Degradation of Organic Pollutants Using Zinc-Iron Selenide. *J. Mol. Liquids* 229, 429–435. doi:10.1016/j.molliq.2016.12.061

Ahmad, K., Naseem, H. A., Parveen, S., Shah, H.-U. -R., Shah, S. S. A., Shaheen, S., et al. (2019). Synthesis and Spectroscopic Characterization of Medicinal Azo Derivatives and Metal Complexes of Indandion. *J. Mol. Struct.* 1198, 126885. doi:10.1016/j.molstruc.2019.126885

Ahmad, A., Mubarak, N. M., Naseem, K., Tabassum, H., Rizwan, M., Najda, A., et al. (2020). Recent Advancement and Development of Chitin and Chitosan-Based Nanocomposite for Drug Delivery: Critical Approach to Clinical Research. *Arabian J. Chem.* 13, 8935–8964. doi:10.1016/j.arabjc.2020.10.019

Ahmad, A., Jini, D., Aravind, M., Parvathiraja, C., Ali, R., Kiyani, M. Z., et al. (2020). A Novel Study on Synthesis of Egg Shell Based Activated Carbon for Degradation of Methylene Blue via Photocatalysis. *Arabian J. Chem.* 13, 8717–8722. doi:10.1016/j.arabjc.2020.10.002

Al-Kordy, H. M. H., Sabry, S. A., and Mabrouk, M. E. M. (2021). Statistical Optimization of Experimental Parameters for Extracellular Synthesis of Zinc Oxide Nanoparticles by a Novel Haloalaliphilic Alkalibacillus sp.W7. *Sci. Rep.* 11, 10924. doi:10.1038/s41598-021-90408-y

Almehizia, A. A., Al-Omar, M. A., Naglah, A. M., Bhat, M. A., and Al-Shakliah, N. S. (2021). Facile Synthesis and Characterization of ZnO Nanoparticles for Studying Their Biological Activities and Photocatalytic Degradation Properties toward Methylene Blue Dye. *Alexandria Eng. J.* 61, 2386–2395. doi:10.1016/j.aej.2021.06.102

Alosman, M., Cao, L., Massey, I. Y., and Yang, F. (2021). The Lethal Effects and Determinants of Microcystin-LR on Heart: A Mini Review. *Toxin Rev.* 40, 517–526. doi:10.1080/15569543.2019.1711417

Anju Chanu, L., Joychandra Singh, W., Jugeshwar Singh, K., and Nomita Devi, K. (2019). Effect of Operational Parameters on the Photocatalytic Degradation of Methylene Blue Dye Solution Using Manganese Doped ZnO Nanoparticles. *Results Phys.* 12, 1230–1237. doi:10.1016/j.rinp.2018.12.089

Bandeira, M., Giovanela, M., Roesch-Ely, M., Devine, D. M., and da Silva Crespo, J. (2020). Green Synthesis of Zinc Oxide Nanoparticles: A Review of the Synthesis Methodology and Mechanism of Formation. *Sust. Chem. Pharm.* 15, 100223. doi:10.1016/j.scp.2020.100223

Bashir, M. S., Jiang, X., Li, S., and Kong, X. Z. (2019). Highly Uniform and Porous Polyurea Microspheres: Clean and Easy Preparation by Interface Polymerization, Palladium Incorporation, and High Catalytic Performance for Dye Degradation. *Front. Chem.* 7, 314. doi:10.3389/fchem.2019.00314

Bashir, M. S., Jiang, X., and Kong, X. Z. (2020). Porous Polyurea Microspheres with Pd Immobilized on Surface and Their Catalytic Activity in 4-nitrophenol Reduction and Organic Dyes Degradation. *Eur. Polym. J.* 129, 109652. doi:10.1016/j.eurpolymj.2020.109652

Biswas, B. D., Purkayastha, M. D., Tiwari, E., Denrah, S., Sarkar, M., Darbha, G. K., et al. (2021). Study of the Photocatalytic Activity of Mn-Doped ZnO Nanocomposites Depending on Their Morphology and Structure with the Variation of Manganese Concentration. *Surf. Inter.* 23, 100902. doi:10.1016/j.surfin.2020.100902

Braydich-Stolle, L., Hussain, S., Schlager, J. J., and Hofmann, M.-C. (2005). *In Vitro* cytotoxicity of Nanoparticles in Mammalian Germline Stem Cells. *Toxicol. Sci. : official J. Soc. Toxicol.* 88, 412–419. doi:10.1093/toxsci/kfi256

Chouke, P. B., Potbhare, A. K., K. Potbhare, A., S. Bhusari, G., Somkuwar, S., Pmd Shaik, D., et al. (2019). Green Fabrication of Zinc Oxide Nanospheres by Aspidopterys Cordata for Effective Antioxidant and Antibacterial Activity. *Adv. Mater. Lett.* 10, 355–360. doi:10.5185/amlett.2019.2235

Czyżowska, A., and Barbasz, A. (2020). A Review: Zinc Oxide Nanoparticles - Friends or Enemies? *Int. J. Environ. Health Res.*, 1–17. doi:10.1080/09603123.2020.1805415

Duman, Ş., Bulut, B., and Özkal, B. (2020). Püskürtmeli Kurutma Ve Ardından Termal Bozunma Ile Sentezlenen Mn Katkılı ZnO Nanotozların Antibakteriyel Ve Optik Özellikleri. *Çukurova Üniversitesi Mühendislik-Mimarlık Fakültesi Dergisi* 35, 1073–1082. doi:10.21605/cukurovaummfd.869176

Dutta, T., Sarkar, R., Pakhira, B., Ghosh, S., Sarkar, R., Barui, A., et al. (2015). ROS Generation by Reduced Graphene Oxide (rGO) Induced by Visible Light Showing Antibacterial Activity: Comparison with Graphene Oxide (GO). *RSC Adv.* 5, 80192–80195. doi:10.1039/c5ra14061g

Fang, Z., Wang, Y., Xu, D., Tan, Y., and Liu, X. (2004). Blue Luminescent center in ZnO Films Deposited on Silicon Substrates. *Opt. Mater.* 26, 239–242. doi:10.1016/j.optmat.2003.11.027

Frank, L. A., Onzi, G. R., Morawski, A. S., Pohlmann, A. R., Guterres, S. S., and Contri, R. V. (2020). Chitosan as a Coating Material for Nanoparticles Intended for Biomedical Applications. *Reactive Funct. Polym.* 147, 104459. doi:10.1016/j.reactfunctpolym.2019.104459

Gul, S., Rehan, Z. A., Khan, S. A., Akhtar, K., Khan, M. A., Khan, M. I., et al. (2017). Antibacterial PES-CA-Ag2O Nanocomposite Supported Cu Nanoparticles Membrane toward Ultrafiltration, BSA Rejection and Reduction of Nitrophenol. *J. Mol. Liquids* 230, 616–624. doi:10.1016/j.molliq.2016.12.093

Han, X., Xu, K., Taratula, O., and Farsad, K. (2019). Applications of Nanoparticles in Biomedical Imaging. *Nanoscale* 11, 799–819. doi:10.1039/c8nr07769j

Ismail, M., Khan, M. I., Khan, S. B., Akhtar, K., Khan, M. A., and Asiri, A. M. (2018). Catalytic Reduction of Picric Acid, Nitrophenols and Organic Azo Dyes via Green Synthesized Plant Supported Ag Nanoparticles. *J. Mol. Liquids* 268, 87–101. doi:10.1016/j.molliq.2018.07.030

Jang, E. S., Khan, S. B., Seo, J., Nam, Y. H., Choi, W. J., Akhtar, K., et al. (2011). Synthesis and Characterization of Novel UV-Curable Polyurethane-Clay Nanohybrid: Influence of Organically Modified Layered Silicates on the Properties of Polyurethane. *Prog. Org. Coat.* 71, 36–42. doi:10.1016/j.porgcoat.2010.12.007

Kamal, T., Khan, S. B., Haider, S., Alghamdi, Y. G., and Asiri, A. M. (2017). Thin Layer Chitosan-Coated Cellulose Filter Paper as Substrate for Immobilization of Catalytic Cobalt Nanoparticles. *Int. J. Biol. Macromolecules* 104, 56–62. doi:10.1016/j.ijbiomac.2017.05.157

Karmakar, M., Mondal, O., Roy, B., Paul, P. K., and Pal, M. (2013). Effect of Mn Doping on Microstructure and Optical Properties of Nanocrystalline ZnO. *Nano* 08, 1350058. doi:10.1142/s1793292013500586

Khan, S. A., Khan, S. B., Kamal, T., Asiri, A. M., and Akhtar, K. (2016b). Recent Development of Chitosan Nanocomposites for Environmental Applications. *Recent Patents on Nanotechnology* 10, 181–188. doi:10.2174/1872210510666160429145339

Khan, S. B., Karimov, K. S., Chani, M. T. S., Asiri, A. M., Akhtar, K., and Fatima, N. (2015). Impedimetric Sensing of Humidity and Temperature Using CeO2-Co3O4 Nanoparticles in Polymer Hosts. *Microchim Acta* 182, 2019–2026. doi:10.1007/s00604-015-1529-1

Khan, S. B., Alamry, K. A., Bifari, E. N., Asiri, A. M., Yasir, M., Gzara, L., et al. (2015). Assessment of Antibacterial Cellulose Nanocomposites for Water Permeability and Salt Rejection. *J. Ind. Eng. Chem.* 24, 266–275. doi:10.1016/j.jiec.2014.09.040

Khan, S. B., Khan, S. A., Marwani, H. M., Bakhsh, E. M., Anwar, Y., Kamal, T., et al. (2016a). Anti-Bacterial PES-Cellulose Composite Spheres: Dual Character toward Extraction and Catalytic Reduction of Nitrophenol. *RSC Adv.* 6, 110077–110090. doi:10.1039/c6ra21626a

Khan, S. A., Shahid, S., Bashir, W., Kanwal, S., and Iqbal, A. (2017). Synthesis, Characterization and Evaluation of Biological Activities of Manganese-Doped Zinc Oxide Nanoparticles. *Trop. J. Pharm. Res.* 16, 2331–2339. doi:10.4314/tjpr.v16i10.4

Khan, N. A., Najam, T., Shah, S. S. A., Hussain, E., Ali, H., Hussain, S., et al. (2020). Development of Mn-PBA on GO Sheets for Adsorptive Removal of Ciprofloxacin from Water: Kinetics, Isothermal, Thermodynamic and Mechanistic Studies. *Mater. Chem. Phys.* 245, 122737. doi:10.1016/j.matchemphys.2020.122737

Kim, D., Jung, J., Kim, Y., Lee, M., Seo, J., and Khan, S. B. (2016). Structure and thermal Properties of Octadecane/expanded Graphite Composites as Shape-Stabilized Phase Change Materials. *Int. J. Heat Mass Transfer* 95, 735–741. doi:10.1016/j.ijheatmasstransfer.2015.12.049

Lang, J., Han, Q., Li, C., Yang, J., Li, X., Yang, L., et al. (2010). Effect of Mn Doping on the Microstructures and Photoluminescence Properties of CBD Derived ZnO Nanorods. *Appl. Surf. Sci.* 256, 3365–3368. doi:10.1016/j.apsusc.2009.12.035

Lee, K. M., Lai, C. W., Ngai, K. S., and Juan, J. C. (2016). Recent Developments of Zinc Oxide Based Photocatalyst in Water Treatment Technology: A Review. *Water Res.* 88, 428–448. doi:10.1016/j.watres.2015.09.045

Mesaros, A., Vasile, B. S., Toloman, D., Pop, O. L., Marinca, T., Unguresan, M., et al. (2019). Towards Understanding the Enhancement of Antibacterial Activity in Manganese Doped ZnO Nanoparticles. *Appl. Surf. Sci.* 471, 960–972. doi:10.1016/j.apsusc.2018.12.086

Nazir, M. A., Khan, N. A., Cheng, C., Shah, S. S. A., Najam, T., Arshad, M., et al. (2020). Surface Induced Growth of ZIF-67 at Co-layered Double Hydroxide: Removal of Methylene Blue and Methyl orange from Water. *Appl. Clay Sci.* 190, 105564. doi:10.1016/j.clay.2020.105564

Pandurangan, M., and Kim, D. H. (2015). *In Vitro* Toxicity of Zinc Oxide Nanoparticles: A Review. *J. Nanopart Res.* 17, 158. doi:10.1007/s11051-015-2958-9

Pathak, T. K., and Swart, H. C. (2019). "Structural and Luminescence Properties of ZnO Nanoparticles Synthesized by Mixture of Fuel Approach in Solution Combustion Method," in *Zinc Oxide Based Nano Materials and Devices* (IntechOpen). doi:10.5772/intechopen.82467

Pathak, T. K., Kumar, A., Swart, C. W., Swart, H. C., and Kroon, R. E. (2016). Effect of Fuel Content on Luminescence and Antibacterial Properties of Zinc Oxide Nanocrystalline Powders Synthesized by the Combustion Method. *RSC Adv.* 6, 97770–97782. doi:10.1039/c6ra22341a

Pryazhnikov, D. V., and Kubrakova, I. V. (2021). Surface-Modified Magnetic Nanoscale Materials: Preparation and Study of Their Structure, Composition, and Properties. *J. Anal. Chem.* 76, 685–706. doi:10.1134/s1061934821060095

Rahman, A-U., Choudhary, M. I., and Thomsen, W. J. (2001). *Bioassay Techniques for Drug Development*. 10.3109/9780203304532: CRC Press.

Shah, S. S. A., Ashfaq, M., Najam, T., Ahmed, M. M., Shaheen, S., Tabassum, R., et al. (2013). Synthesis of Sulfonamides, Metal Complexes and the Study of *In Vitro* Biological Activities. *Curr. Bioactive Comp.* 9, 211–220. doi:10.2174/15734072090314011952646

Sharma, N., Jandaik, S., Kumar, S., Chitkara, M., and Sandhu, I. S. (2016). Synthesis, Characterisation and Antimicrobial Activity of Manganese- and Iron-Doped Zinc Oxide Nanoparticles. *J. Exp. Nanoscience* 11, 54–71. doi:10.1080/17458080.2015.1025302

Singh, A., Singh, N. B., Afzal, S., Singh, T., and Hussain, I. (2018). Zinc Oxide Nanoparticles: a Review of Their Biological Synthesis, Antimicrobial Activity, Uptake, Translocation and Biotransformation in Plants. *J. Mater. Sci.* 53, 185–201. doi:10.1007/s10853-017-1544-1

Singh, J., Rathi, A., Rawat, M., Kumar, V., and Kim, K.-H. (2019). The Effect of Manganese Doping on Structural, Optical, and Photocatalytic Activity of Zinc Oxide Nanoparticles. *Composites B: Eng.* 166, 361–370. doi:10.1016/j.compositesb.2018.12.006

Sonkusare, V. N., Chaudhary, R. G., Bhusari, G. S., Rai, A. R., and Juneja, H. D. (2018). Microwave-Mediated Synthesis, Photocatalytic Degradation and Antibacterial Activity Ofα-Bi 2 O 3 Microflowers/novelγ-Bi 2 O 3 Microspindles. *Nano-Structures & Nano-Objects* 13, 121–131. doi:10.1016/j.nanoso.2018.01.002

Taloni, A., Vodret, M., Costantini, G., and Zapperi, S. (2018). Size Effects on the Fracture of Microscale and Nanoscale Materials. *Nat. Rev. Mater.* 3, 211–224. doi:10.1038/s41578-018-0029-4

Tănase, M. A., Soare, A. C., Oancea, P., Răducan, A., Mihăescu, C. I., Alexandrescu, E., et al. (2021). Facile *In Situ* Synthesis of ZnO Flower-Like Hierarchical Nanostructures by the Microwave Irradiation Method for Multifunctional Textile Coatings. *Nanomaterials* 11, 2574. doi:10.3390/nano11102574

Thakur, D., Sharma, A., Awasthi, A., Rana, D. S., Singh, D., Pandey, S., et al. (2020). Manganese-Doped Zinc Oxide Nanostructures as Potential Scaffold for Photocatalytic and Fluorescence Sensing Applications. *Chemosensors* 8, 120. doi:10.3390/chemosensors8040120

Vinci, G., and Rapa, M. (2019). *Noble Metal Nanoparticles Applications: Recent Trends in Food Control*. Basel, Switzerland: Bioengineering, 6.

Yang, M., Guo, Z., Qiu, K., Long, J., Yin, G., Guan, D., et al. (2010). Synthesis and Characterization of Mn-Doped ZnO Column Arrays. *Appl. Surf. Sci.* 256, 4201–4205. doi:10.1016/j.apsusc.2010.01.125

Zhan, M., Hussain, S., AlGarni, T. S., Shah, S., Liu, J., Zhang, X., et al. (2021). Facet Controlled Polyhedral ZIF-8 MOF Nanostructures for Excellent NO2 Gas-Sensing Applications. *Mater. Res. Bull.* 136, 111133. doi:10.1016/j.materresbull.2020.111133

Conflict of Interest: The authors declare that the research was conducted in the absence of any commercial or financial relationships that could be construed as a potential conflict of interest.

Publisher's Note: All claims expressed in this article are solely those of the authors and do not necessarily represent those of their affiliated organizations, or those of the publisher, the editors, and the reviewers. Any product that may be evaluated in this article or claim that may be made by its manufacturer is not guaranteed or endorsed by the publisher.